Journal of Applied Electrochemistry **31**: 953–959, 2001.

Extending the life of maintenance-free lead/acid batteries by etching of grids in sodium hydroxide

R. DE MARCO*, A. ROCHLIADI and J. JONES
School of Applied Chemistry, Curtin University of Technology, GPO Box U 1987, Perth, Western Australia, 6845, Australia
*(*author for correspondence)*

Received 29 September 2000; accepted in revised form 2 May 2001

Key words: grid corrosion layer, lead/acid battery, plate passivation, positive active material, premature capacity loss

Abstract

The surfaces of lead–calcium–tin grids etched in NaOH have been characterized by using X-ray photoelectron spectroscopy (XPS) and environmental scanning electron microscopy (ESEM). It is shown that the basic lead carbonate phase, hydrocerussite, present on the surfaces of lead–calcium–tin grids is removed via etching in NaOH, due presumably to the dissolution of lead(II) salts as water soluble lead(II) complexes. Charge/discharge cycling data for non-antimonial batteries fabricated by using untreated and grid etched 2 V cells have demonstrated that the removal of grid surface hydrocerussite diminishes the rate of premature capacity loss displayed by non-antimonial batteries in the early stages of cycling. Furthermore, scanning electron microscopy (SEM) of the corrosion layers of positive plates for untreated and grid etched cells, in the initial stages of cycling, demonstrated that the removal of grid surface hydrocerussite ameliorates the problem caused by passivation of the grid corrosion layer through the formation of an uninterrupted underlayer of PbO.

1. Introduction

Although a major cause of premature capacity loss (PCL) in lead/acid batteries involves the disintegration of interparticle networks in the positive active material (PAM) according to the agglomerate of spheres model [1–9], there is ample evidence that grid corrosion and its concomitant effect on increasing the resistance of the grid–corrosion layer interface has a deleterious effect on the durability of lead/acid batteries [10–21], albeit that the latter phenomenon is generally considered to be less problematic [1, 6].

Recent work [17] has demonstrated that the presence of deliberately invoked basic lead carbonate, hydrocerussite, on non-antimonial grids has a detrimental effect on the charge/discharge cycling behaviour of lead/acid batteries, and this phenomenon is presumably underpinned by the grid corrosion pattern taking place beneath the grid surface layer of hydrocerrusite [16]. Furthermore, a recent study [18] involving the characterization of non-antimonial grid corrosion layers by X-ray photoelectron spectroscopy (XPS) revealed that the initial overcharging of cells, which is symbolic of cell polarization through grid corrosion, is associated with the development of a bilayer corrosion film comprising a thin underlayer of PbO, along with a thick overlayer of PbO_2. Clearly, the presence of an insulating underlayer of PbO is expected to block the transfer of charge to the current collecting grid, thereby giving rise to an alternate form of PCL, as has been demonstrated elsewhere in the literature [17].

The previous work [16–18] strongly suggests that employing a suitable grid etching and plate preparation process that removes grid hydrocerussite, and prevents its reformation, may ameliorate PCL caused by grid hydrocerussite-induced PbO formation. It is well known that all lead(II) salts will dissociate into highly soluble lead complexes (i.e., $Pb(OH)^+$ and $Pb_4(OH)_4^{4+}$) under alkaline conditions [22], so it is technically feasible to remove grid hydrocerussite via the etching of grids in strongly alkaline solutions (e.g., 10% w/v NaOH). Importantly, the presence of residual amounts of etcher in plates after the treatment of grids in NaOH is unproblematic, as Na^+ ions are electrochemically inert under the charging conditions of lead/acid batteries. Furthermore, the need to prevent the reformation of grid surface hydrocerussite during the subsequent processing of plates precludes the use of normal plate curing conditions (i.e., high temperature and high humidity for prolonged periods). Notably, a recent US Patent [23] demonstrated that cureless plates of high integrity may be prepared by employing the common battery making practices of wringing of wet plates between adsorbent material and/or flash drying of plates in a naked flame

and, for reasons of simplicity and ease of control, the authors have opted for the former procedure. Consequently, a combination of grid etching in NaOH, along with the use of a cureless plate preparation process, is deemed suitable for amelioration of the deleterious effects associated with grid surface hydrocerussite.

The aim of this study was to develop a grid etching and plate preparation process that removes hydrocerussite from native grid surfaces, and prevents its reformation. This has necessitated the characterisation of non-antimonial grid surfaces, aged for long periods in humidified ovens to promote the formation of copious amounts of hydrocerussite, before and after etching in 10% w/v NaOH by using XPS and environmental scanning electron microscopy (ESEM). Furthermore, the implications of the new plate preparation procedure on PCL in non-antimonial lead/acid batteries has been ascertained by subjecting control and etched grid 2 V cells to cycle-life tests by using repetitive charge/discharge cycling. The impact of grid etching on the corrosion layers of non-antimonial grid positive plates has also been investigated by using scanning electron microscopy (SEM).

2. Experimental details

2.1. *XPS/ESEM analysis of grids*

XPS spectra were recorded by using a modified AEI ES 100 spectrometer that employs a near monoenergetic AlK_α X-ray source, and an analyser chamber pressure of 10^{-10} hPa. All measured atomic core-level binding energies were determined by using Au($4f_{7/2}$) and C(1s) peaks at 83.98 and 284.6 eV, respectively [24]. Atomic ratios and corresponding surface stoichiometries were derived by using photoelectron line intensities in conjunction with the empirical atomic sensitivity factors of Wagner et al. [25].

ESEM work was undertaken by using the Electroscan ESEM(S)E-3 instrument available at the electron microscopy centre at The University of Western Australia. An accelerating voltage of 30 kV, and a spot size of 40, were employed in the measurement of all images. The chamber pressure in the ESEM was 1.2 torr.

2.2. *SEM analysis of grid corrosion layers*

The grid corrosion layers of epoxy-mounted, polished cross sections of positive plates were examined by SEM using a Phillips XL30 electron microscope operated at an accelerating voltage of 25 kV, and a spot size setting of 4. The specimens were ground successively on 500, 1000 and 1200 grit emery paper by using a paraffin lubricant and a Struers Dap-V disc polisher that was rotated at 300 rpm. After grinding, the specimens were polished successively on Struers DP-Spray, P diamond sprays (3 and 1 μm) that had been applied to DP-Nap and DP-Mol felt pad discs using a rotation speed of 300 rpm and the Struers DP-lubricant Red.

2.3. *Assembly and charge/discharge cycling of 2 V cells*

Cureless untreated and grid etched, along with cured untreated hand pasted positive plates were assembled into 2 V cells, comprising one positive plate surrounded by two factory produced negative plates, by using the materials and procedures that have been described elsewhere by the authors [17, 18]. It is important to note that lead–calcium–tin grids have been used in the fabrication of positive plates.

It was deemed necessary to use a cureless plate preparation to avoid the regeneration of grid hydrocerussite during the curing of plates prepared by using grids that were etched in 10% w/v NaOH for 30 min. To improve the integrity of the pasted material, four lead bricks (each weighing 11 kg) were stacked on top of six plates that were individually wrapped in one absorptive glass mat separator, and sandwiched as a stack between two metal plates. The battery plate stack was pressed for 45 min before replacing the glass mat separators with fresh ones, and pressing for another 45 min. Notably, the cohesive strength of active material in cureless plates, as estimated by measuring the weight loss accompanying the dropping of several plates from a height of 3 m, was similar to the corresponding cohesive strength of cured active material.

The cycle-life performance of 2 V cells was assessed by employing a Digatron BTS-500 computerized charge/discharge unit (Digatron GmbH, Germany) to undertake repetitive charge/discharge cycling at the 3 h rate. After charging to 2.55 V at a constant current of 5.6 A, the cells were held at the top-of-charge voltage (TOCV) until the current had tapered to 1 A. At this juncture, the cells were discharged at a constant current of 5.6 A until the voltage dropped to 1.75. The charge/discharge procedure was repeated until the discharge capacity fell to 50% of its original value.

Previous work [17] has demonstrated that this self-regulating charge/discharge cycling regime avoids the imposition of high overpotentials (i.e., 2.8–2.9 V) and the use of trickle currents during charging, as employed in conventional two-step constant current charging regimes, and these factors conspire to accelerate the rate of PCL in the early stages of cycling. This approach was used to accentuate or amplify the subtle effects of grid etching on the rate of PCL for non-antimonial batteries.

3. Results and discussion

A lead–calcium–tin grid, comprising 0.098 wt % Ca and 0.42 wt % Sn [16], that had been polished on 1200 grit silicon carbide paper was aged at 50 °C and high humidity for four weeks in order to promote the formation of copious amounts of hydrocerussite that

are detectable using surface analysis techniques [16]. This humidified grid was characterized by using XPS and ESEM before and after etching in 10% w/v NaOH for 30 min. The purpose of this experiment was to assess the efficacy of grid etching in NaOH under worst case conditions of grids possessing a relatively thick overlayer of hydrocerussite.

3.1. *XPS analysis of grids*

In a previous study [16], the surface layers of a variety of non-antimonial grids were characterised by using XPS and X-ray diffraction (XRD). The results demonstrated that hydrocerussite is present on the surfaces of as-received grids, due presumably to the aerial oxidation of lead, along with its concomitant degradation to $2PbCO_3 \cdot Pb(OH)_2$ (i.e., hydrocerussite) in the presence of atmospheric carbon dioxide.

Respectively, Figures 1(a)–3(a) present XPS spectra for the Pb(4f), O(1s) and C(1s) levels of a lead–calcium–tin grid that has been aged in a humidified oven for four weeks. The Pb(4f) spectrum revealed the characteristic spin-orbit split components at binding energies of 138.3 eV and 143.4 eV (Table 1) that are indicative of Pb in PbO, PbO_2 and/or $Pb(OH)_2$ [26], while the O(1s) binding energy of 530.5 eV is attributable to O^{2-}, OH^- or CO_3^{2-}, or a combination of the above-mentioned oxygen species [26]. The C(1s) spectrum showed a major peak at 284.6 eV (Table 1) that is due to adventitious hydrocarbons in the XPS system, while the high binding energy peak at 288.6 eV (Table 1) is symbolic of CO_3^{2-} in lead carbonate [26, 27].

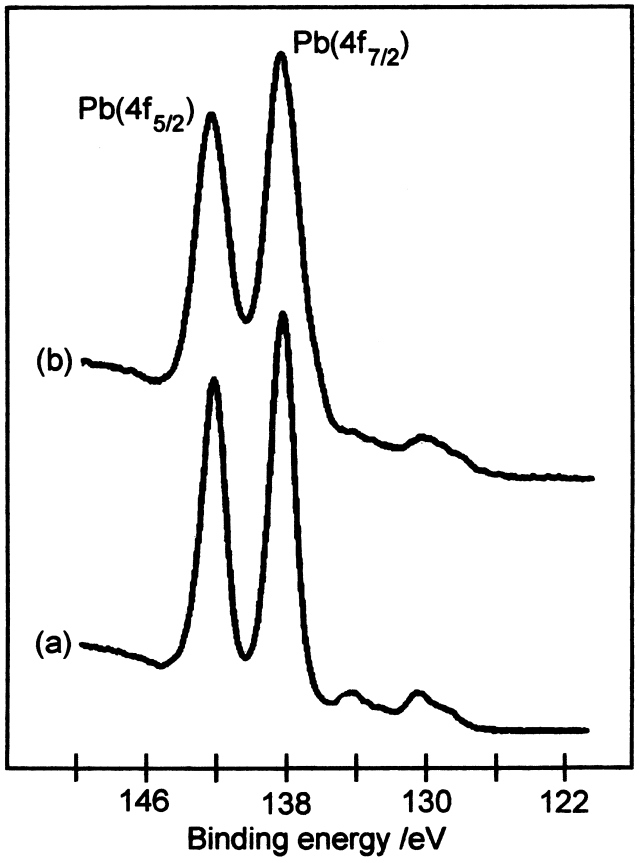

Fig. 1. XPS spectra of the Pb(4f) level for the following sample: (a) an untreated lead–calcium–tin grid exposed to 50 °C and high humidity for four weeks; and (b) the humidified grid after etching in 10% w/v NaOH for 30 min.

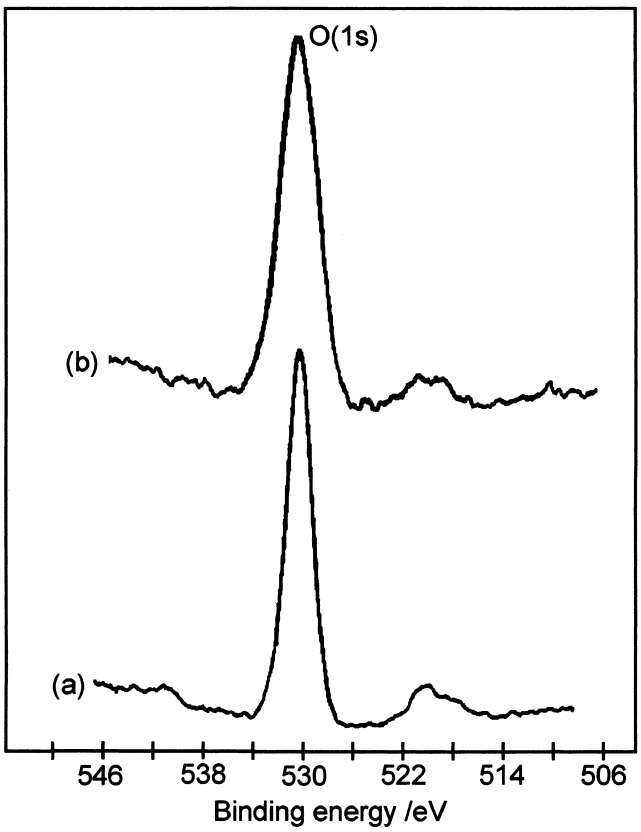

Fig. 2. XPS spectra of the O(1s) level for the following sample: (a) an untreated lead–calcium–tin grid exposed to 50 °C and high humidity for four weeks; and (b) the humidified grid after etching in 10% w/v NaOH for 30 min.

Figures 1(b)–3(b) and Table 1, respectively, present XPS spectral and binding energy data for the Pb(4f), O(1s) and C(1s) levels of a humidified grid after etching in 10% w/v NaOH for 30 min. The Pb(4f) and O(1s) spectra did not reveal any discernible chemical shifts, symbolising that lead and oxygen species on the etched grid surface are very similar to those of the humidified grid. By contrast, the C(1s) level for the NaOH-etched grid revealed a disappearance of the high binding energy lead carbonate peak at about 289 eV, while the small shoulder at about 286 eV is attributable to the presence of adsorbed CO_2 [28].

Figure 4 presents XPS spectra of the Sn(3d) and Zr(3p) levels for a humidified lead–calcium–tin grid that was etched in 10% w/v NaOH for 30 min. Note that the humidified grid surface did not reveal the presence of tin and zirconium. The $Sn(3d_{5/2})$ and $Sn(3d_{3/2})$ spin-orbit split components at 485.1 eV and 493.5 eV are indicative of SnO [26], while the $Zr(3p_{3/2})$ and $Zr(3p_{1/2})$ peaks at 332.3 eV and 345.8 eV are symbolic of ZrO_2 [26]. In a previous study [16], it was noted that the elemental concentration of tin in the oxidised surface layers of

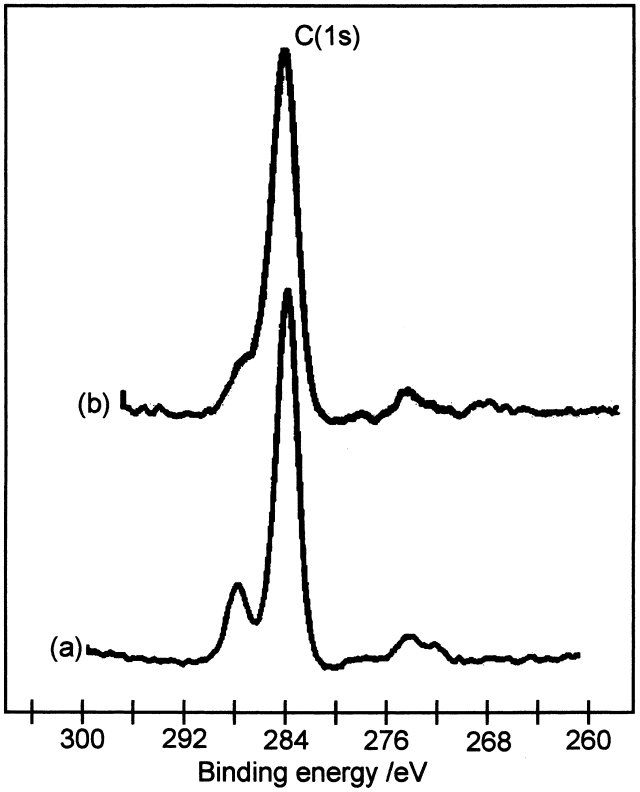

Fig. 3. XPS spectra of the C(1s) level for the following sample: (a) an untreated lead–calcium–tin grid exposed to 50 °C and high humidity for four weeks; and (b) the humidified grid after etching in 10% w/v NaOH for 30 min.

Table 1. XPS binding energies/eV of core atomic energy levels for Pb, C, Sn and Zr for a non-antimonial grid subjected to different treatments

Level	Pb–Ca–Sn grid aged in a humidified oven*	Pb–Ca–Sn grid aged in a humidified oven and etched in 10% w/v NaOH†
$Pb(4f_{7/2})$	138.3	138.3
$Pb(4f_{5/2})$	143.4	143.6
C(1s)	284.6; 288.6	284.6
O(1s)	530.5	529.8
$Sn(3d_{5/2})$	nd	485.1
$Sn(3d_{3/2})$	nd	493.5
$Zr(3p_{3/2})$	nd	332.3
$Zr(3p_{1/2})$	nd	345.8

nd = not detected.
*ageing at 50 °C, high humidity for four weeks.
†ageing at 50 °C, high humidity for four weeks plus etching for 30 min.

as-received non-antimonial grids was approximately 1–2 orders of magnitude higher than the corresponding bulk elemental concentrations, due presumably to the enrichment and preferential oxidation of tin that had precipitated at the grain boundaries at bulk tin concentrations above the room temperature solid solubility in lead [29]. The untreated humidified grid did not reveal a surface preconcentration of tin, as the formation of copious amounts of hydrocerussite had obviously encapsulated the SnO deposits; however, etching of the humidified

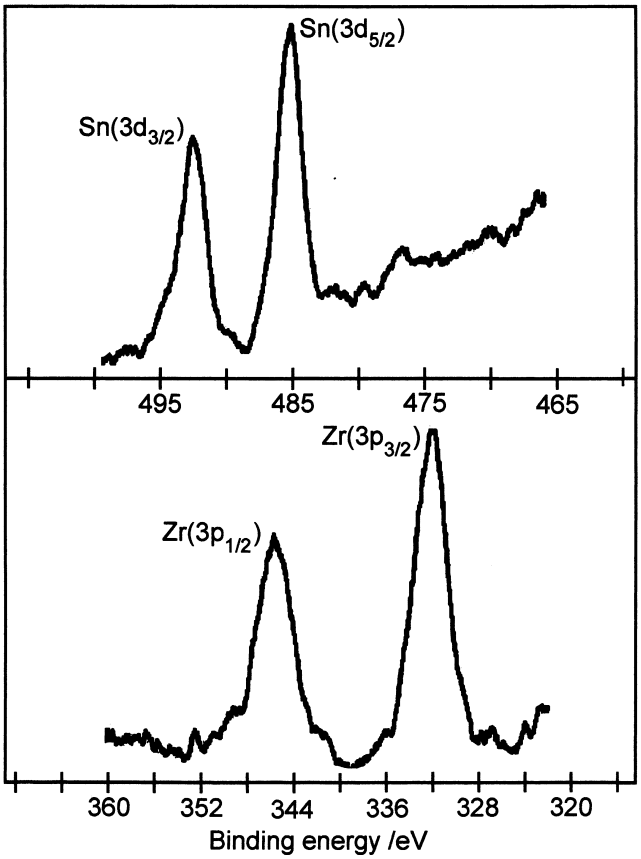

Fig. 4. XPS spectra for (a) Sn(3d) and (b) Zr(3p) levels for an untreated lead–calcium–tin grid exposed to 50 °C and high humidity for four weeks, after etching in 10% w/v NaOH for 30 min.

grid in NaOH revealed the underlying SnO deposits, and the XPS surface concentration of tin was found to be 13 wt %. This outcome has important ramifications for the cycle-life of non-antimonial batteries fabricated by using grids that have been etched in NaOH; the removal of hydrocerussite will ameliorate the passivation of positive grid corrosion layers by PbO in non-antimonial batteries, and the formation of a tin enriched surface layer is expected to improve battery durability, as it is well known that the cycle-life of non-antimonial batteries increases as a function of grid tin content due to the precipitation of conductive tin oxide at the grain boundaries of PbO, which progressively diminishes the rate of growth of PbO in the positive grid corrosion layer [19]. Although the exact source of the ZrO_2 impurity is unknown, it is very likely that it originates from the releasing agent (a slurry composed of a variety of constituents, including low grade silica which is likely to be contaminated by ZrO_2) that is used in the prevention of sticking of alloys to moulds during the casting of grids.

3.2. *ESEM examination of grids*

The XPS data in the previous section demonstrated that grid etching in 10% w/v NaOH removes all grid surface hydrocerussite. This work was conducted necessarily

under *ex situ* and ultrahigh-vacuum conditions by using samples that had been rinsed in distilled water, and these conditions do not mimic those of wet grid surfaces (by NaOH) that are encountered during plate pasting. By contrast, ESEM is capable of providing high-resolution images of wet surfaces that are indeed representative of the grid surfaces encountered during plate pasting.

The ESEM secondary electron micrograph for an as received grid (Figure 5(a)) revealed crystalline deposits of detrimental hydrocerussite, as has been observed elsewhere [16], while the wet and unrinsed NaOH-etched specimen (Figure 5(b)) revealed an extensively roughened grid topography that is expected for a surface layer of crystalline deposits of hydrocerussite that have been attacked severely by chemical etching in 10% w/v NaOH.

The aforementioned XPS and ESEM surface analysis results demonstrate that grid etching in NaOH is an efficacious method that removes and prevents the reformation of detrimental grid surface hydrocerussite.

3.3. *Battery cycling results*

This part of the work was conducted using as-received grids that were etched in 10% w/v NaOH to assess the implications of the removal of native grid surface hydrocerussite on the charge/discharge cycling properties of non-antimonial lead/acid batteries. Note that battery plants commonly paste grids within 1–3 days of casting, and this period of exposure to the atmosphere is likely to cause aerial oxidation of the lead surface to PbO and a concomitant alteration of the oxide film to hydrocerussite, as shown elsewhere by using XPS [16]. Nevertheless, it must be acknowledged that battery production processes employing expanded or continuously cast grids, whereby the automatic process ensures the almost instantaneous pasting of grids, is unlikely to generate a thick layer of hydrocerussite, and the NaOH etching process is not expected to exert a significant influence on the charge/discharge cycling characteristics of these batteries.

The average charge/discharge cycling data (acquired by the present author (J.J.) in 1997) for the following plates are presented in Figure 6(a): (●) 6 cured and untreated plates; (▲) 12 cureless and untreated plates; and (■) 12 cureless and grid etched plates. Also, the average charge/discharge cycling data (acquired by the present author (A.R.) in 2000) for (▲) 10 cureless and untreated plates, along with (●) 10 cureless and grid etched cells are presented in Figure 6(b). Clearly, these independent yet identical experiments illustrate the large uncertainties inherent to charge/discharge cycling data (viz., 10–20% relative), and the limitations of these large

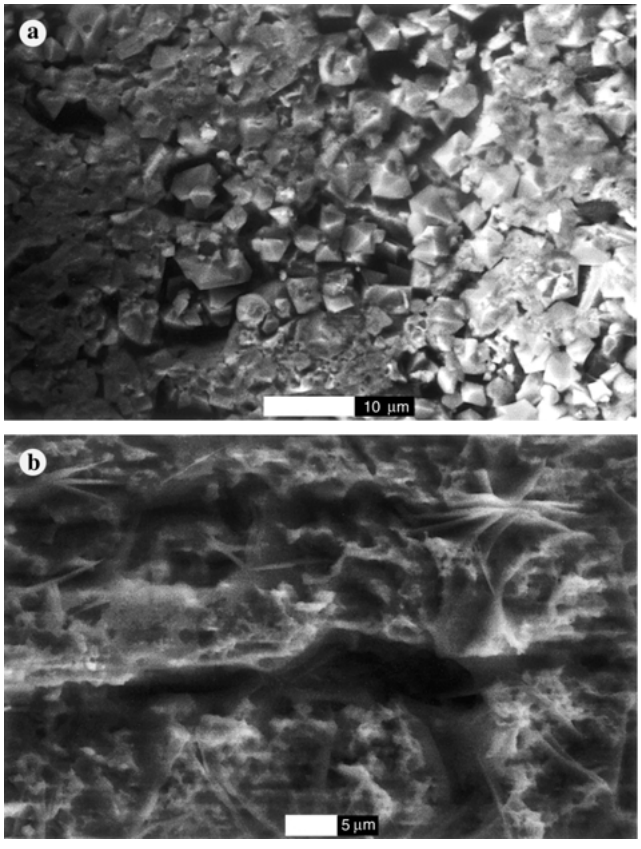

Fig. 5. ESEM secondary electron micrographs of (a) a humidified lead–calcium–tin battery grid, and (b) a humidified lead–calcium–tin battery grid etched in 10% w/v NaOH for 30 min.

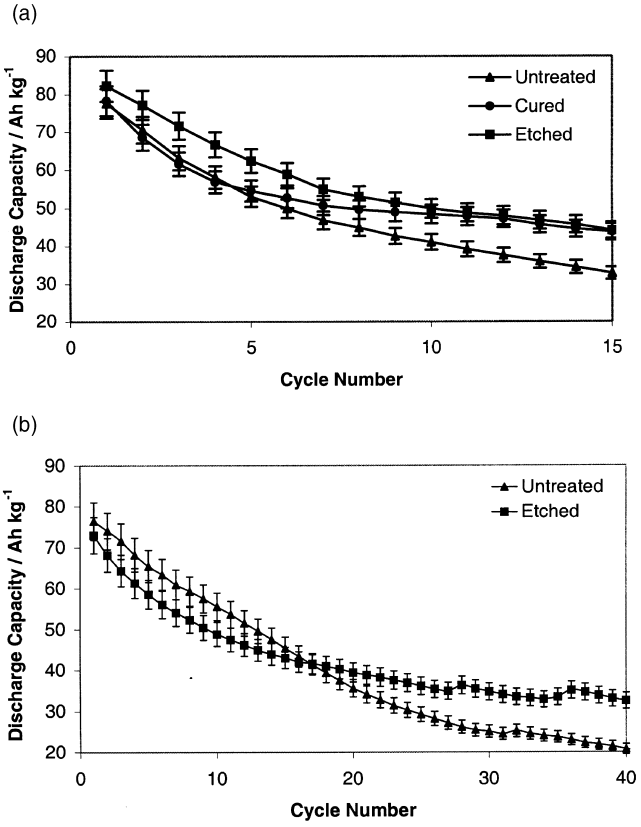

Fig. 6. Discharge capacity data/Ah kg^{-1} for 2 V non-antimonial cells subjected to charge/discharge cycling: (a) 6 cured and untreated plates (●), 12 cureless and untreated plates (▲), and 12 cureless and grid etched plates (■); and (b) 10 cureless and untreated plates (▲), along with 10 cureless and NaOH etched grid plates (■).

experimental errors in deriving information about improvements in the efficacy of new battery manufacturing techniques. Nevertheless, it is evident in both data sets that the etching of lead–calcium–tin grids in 10% w/v NaOH reduces the rate of PCL in the early stages of cycling (i.e., in the first 15 cycles). Furthermore, it can also be seen in Figure 6(a) that the cureless and grid etched plates give a slower rate of PCL compared to cured and untreated grid plates, as evidenced by a diminished rate of PCL during the first 10 cycles.

The analysis of variance (ANOVA) statistical test employs an F-test at the 95% confidence limit to ascertain if the variance in datasets for 10 cureless and grid etched, along with 10 cureless and untreated cells is attributable to a random deviation in cycling data, or if there is a statistically significant difference between the two sets of cycling data. Essentially, the F values for the two groups of data (Table 2) exceed the critical F value at the 95% confidence limit, demonstrating that the etching of grids reduces significantly the rate of decline in discharge capacity in the initial stages of cycling (i.e., 10–15 cycles).

In summary, the battery charge/discharge cycling data demonstrate that the etching of positive grids in 10% w/v NaOH influences the structure and properties of the grid corrosion layer/PAM interface, thereby ameliorating the usual rapid PCL that occurs in the initial stages of charge/discharge cycling.

3.4. *SEM characterization of cycled plate materials*

Previous SEM and XPS work [18] revealed an underlayer deposit of insulating PbO in the corrosion layers of cured battery plates prepared using untreated grids after 6 cycles, while the corrosion film formed after 15 cycles comprised a single layer that is composed of a conductive PbO_{2-x}, which involves some Pb^{2+} doping of the PbO_2 lattice. This behaviour is ascribable to the well-known electrochemistry of Pb in which Pb is first oxidized to PbO prior to further oxidation to the non-stoichiometric phase of PbO_{2-x}. It is important to note that previous work [18] has shown that the concomitant cessation in grid corrosion in the later stages of cycling for the conditions used in this study, as evidenced by a diminution in the ratios of capacities for charge-to-discharge, enabled the oxidation of PbO to a near-uniform layer of PbO_{2-x}.

The aforementioned findings strongly support a hypothesis in which hydrocerussite encourages the formation of a thick and uninterrupted underlayer of PbO early in a battery's life [16, 17], degrading the performance of maintenance-free lead/acid batteries. Conversely, the removal of hydrocerussite and the enrichment of conductive tin oxide in the surface layers of NaOH-etched grids decrease the rate of formation of PbO in the positive grid corrosion layer [17, 19], thereby forming a thin and interrupted layer of PbO that is less problematic in the context of charge/discharge cycling of non-antimonial batteries.

In the present work, the authors studied the corrosion layers of cureless plate 2 V cells (after 3 cycles) prepared using untreated and NaOH-etched lead–calcium–tin grids, respectively. The backscattered SEM images (Figure 7(a) and (b)) revealed a classical uninterrupted PbO underlayer in the 4 μm thick corrosion layer of the untreated plate, while the NaOH-etched grid cell did not appear to produce an uninterrupted layer of detrimental PbO in the 4 μm corrosion layer of this plate. Clearly,

Table 2. ANOVA comparative test for untreated against grid etched cells–cycles to 37Ah

ANOVA: single factor for untreated versus grid etched plates

Summary

Groups	Count	Sum	Average	Variance
Untreated	10	200	20	1.555556
Etching	10	252	25.2	24.62222

ANOVA

Source of variation	*SS*	*df*	*MS*	*F*	*P-value*	$F_{critical}$
Between groups	135.2	1	135.2	10.32937	0.004813	4.413863
Within groups	235.6	18	13.08889			
Total	370.8	19				

Because $F > F_{critical}$ there is significant difference between the data.

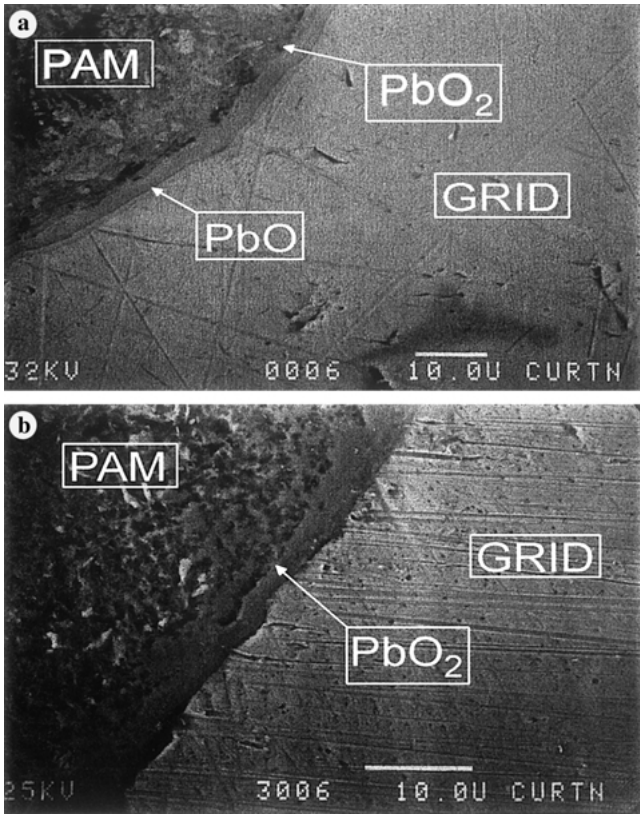

Fig. 7. SEM backscattered electron micrographs of polished cross-sections of non-antimonial lead/acid battery positive plates after 3 cycles: (a) an untreated cureless plate; (b) a NaOH-etched grid cureless plate.

the removal of grid surface hydrocerussite by etching of grids in NaOH ameliorates the concomitant passivation of the grid corrosion layer through the formation of a thick and uninterrupted underlayer of PbO.

4. Conclusions

The XPS results for lead–calcium–tin grids etched in 10% w/v NaOH demonstrate unequivocally that an alkaline grid pretreatment removes detrimental grid hydrocerussite from the surface of non-antimonial grids. The ESEM results for wet grids exposed to NaOH confirm that the alkaline treatment not only removes hydrocerussite, but also prevents its reformation at a wet grid surface (by NaOH) which is exposed to air prior to the pasting of plates.

The charge/discharge cycling data demonstrate that a positive plate preparation process based on the etching of grids in NaOH and the production of cureless plates is capable of reducing the PCL experienced by maintenance-free lead/acid batteries in the early stages of charge/discharge cycling.

The absence of a thick and uninterrupted PbO underlayer in the corrosion layers of NaOH-etched grid positive plates confirms the central hypothesis of this work, that is, amelioration of the hydrocerussite-induced formation of PbO by NaOH etching of grids may extend the life of maintenance-free batteries.

Acknowledgements

The authors thank GNB Battery Technologies for providing the battery materials used in this study, along with the Australian Research Council and Alternative Energy Development Board for financial assistance. We are grateful to Mr Marshall Hughes of the Chemistry Department, University of Tasmania, for assistance with the XPS analyses.

References

1. K.K. Constanti, A.F. Hollenkamp, M.J. Koop and K. McGregor, *J. Power Sources* **55** (1995) 269.
2. A.F. Hollenkamp, K.K. Constanti, M.J. Koop, L. Apateanu, M. Calabek and K. Micka, *J. Power Sources* **48** (1994) 195.
3. A. Winsel, E. Voss and U. Hullmeine, *J. Power Sources* **30** (1990) 209.
4. M. Calabek, K. Micka, P. Baca, P. Krivak and V. Smarda, *J. Power Sources* **62** (1996) 161.
5. P.T. Moseley, *J. Power Sources* **59** (1996) 81.
6. R.H. Newnham and W.G.A. Baldsing, *J. Power Sources* **66** (1997) 27.
7. E. Bashtavelova and A. Winsel, *J. Power Sources* **67** (1997) 93.
8. S. Atlung and T. Jacobsen, *J. Power Sources* **66** (1997) 147.
9. A.F. Hollenkamp, *J. Power Sources* **59** (1996) 87.
10. D. Pavlov, *J. Power Sources* **46** (1993) 171.
11. M.K. Dimitrov and D. Pavlov, *J. Power Sources* **46** (1993) 203.
12. D. Pavlov, *J. Power Sources* **53** (1995) 9.
13. D. Pavlov, *J. Power Sources* **48** (1994) 179.
14. D. Pavlov, A. Dakhouche and T. Rogachev, *J. Appl. Electrochem.* **27** (1997) 720.
15. A. El Ghachcham Amrani, Ph. Steyer, J. Steinmetz, P. Delcroix and G. Le Caer, *J. Power Sources* **64** (1997) 35.
16. R. De Marco and J. Liesegang, *Appl. Surf. Sci.* **84** (1995) 237.
17. R. De Marco, *J. Appl. Electrochem.* **27** (1997) 99.
18. R. De Marco and J. Jones, *J. Appl. Electrochem.* **30** (2000) 77.
19. E. Rocca and J. Steinmetz, *Electrochim. Acta* **44** (1999) 4611.
20. S. Fouache, A. Chabrol, G. Fossati, M. Bassini, M.J. Sainz and L. Atkins, *J. Power Sources* **78** (1999) 12.
21. E.M. Lehockey, D. Limoges, G. Palumbo, J. Sklarchuk, K. Tomantschger and A. Vincze, *J. Power Sources* **78** (1999) 79.
22. F.A. Cotton and G. Wilkinson, 'Advanced Inorganic Chemistry. A Comprehensive Text' (J. Wiley & Sons, New York, 4th edn, 1980).
23. E. Purushothama Rao and F.L. Marsh, *US Patent 4 713 304* (1987) 1.
24. M.P. Seah, *Surf. Interface Anal.* **14** (1989) 488.
25. C.D. Wagner, L.E. Davis, M.V. Zeller, J.A. Taylor, R.M. Raymond and L.H. Gale, *Surf. Interface Anal.* **3** (1981) 211.
26. J.F. Moulder, W.F. Stickle, P.E. Sobol and K.D. Bombden (Eds), 'Handbook of X-ray Photoelectron Spectroscopy' (Perkin-Elmer, Eden Prairie, MN, 1992).
27. V. Young and P.C. McCaslin, *Anal. Chem.* **57** (1985) 880.
28. J.S. Hammond, S.W. Gaarenstroom and N. Winograd, *Anal. Chem.* **47** (1975) 2193.
29. N.E. Bagshaw, *in* T. Kiely and B.W. Baxter (Eds), 'Research and Development in Non-Mechanical Electrical Power Sources, Power Sources 12' (International Power Sources, UK, 1988).